Journal of Applied Fluid Mechanics, Vol. 9, No. 5, pp. 2133-2140, 2016.
Available online at www.jafmonline.net, ISSN 1735-3572, EISSN 1735-3645.
DOI: 10.18869/acadpub.jafm.68.236.25096

Research on the Aerodynamic Lift of Vehicle Windshield Wiper

G. Zhengqi[1,2], C. Zhen[1†] and T. Peng[1]

[1]*State Key Laboratory of Advanced Design and Manufacture for Vehicle Body of Hunan University, Changsha, Hunan, 410082, China*
[2]*Hunan University of Arts and Science, Changde, Hunan, 415000, China*

†*Corresponding Author Email: chenzhen88@hnu.edu.cn*

(Received May 21, 2015; accepted September 8, 2015

ABSTRACT

Currently, research on the aerodynamic lift of vehicle windshield wipers is confined to the steady results, and there are very few test results. In the face of this truth, a wind tunnel test is conducted by using the Multipoint Film Force Test System (MFF). In this test, the aerodynamic lift of four kinds of wiper is measured at different wind speeds and different rotation angles. And then, relevant steady-state numerical simulations are accomplished and the mechanism of the aerodynamic lift is analyzed. Furthermore, combined with dynamic meshing and user-defined functions (UDF), transient aerodynamic characteristics of wipers are obtained through numerical simulations. It is found that the aerodynamic lift takes great effect on the stability of wipers, and there is maximum value of the lift near a certain wind speed and rotation angle. The lift force when wipers are rotating with the free stream is less than steady, and the force when rotating against the free stream is greater than steady.

Keywords: Windshield wiper; Aerodynamic lift; Wind tunnel test; Dynamic mesh; UDF.

NOMENCLATURE

ρ	fluid density	u_g	moving speed of the mesh
μ	turbulent viscosity	Γ	diffusion coefficient
x_i	component of the axis in the x direction	S_φ	source term of φ
x_j	component of the axis in the y direction	u	velocity vector
τ_{ij}	subgrid-scale stress	V	control volume
δ_{ij}	kronecker delta	S_{ij}	resolved strain rate tensor
e	error		

1. INTRODUCTION

In order to reduce the negative effect on driving performance brought by rain， a windshield wiper was proposed (Anderson 1903; Frédéric *et al.* 2014). Influenced by the airflow when the vehicle is moving, the windshield wiper is subjected to aerodynamic lift force, which is exerted perpendicular to the windshield. The wiper will float when its preload force is not powerful enough to counteract the aerodynamic lift force, which will directly cause the rainwater not to be brushed away completely (Shibata and Sakoda 1979; Takada *et al.* 2003). And then, the driver's vision is partially obstructed, which will result in traffic accidents. The floating phenomenon also has a bad effect on the wiper's service life. And, adding too much pre tightening force increases the friction between rubber and glass, which is a primary factor in inducing squeal noises from vehicle wiper systems on automotive windshields (Sanon and Jallet 2003; Ali *et al.* 2013; Dongki *et al.* 2014). Meanwhile, excessive preload force also increases motor load and scratches the windshield. Considering of the above situation, the best solution is to reduce the aerodynamic lift of wipers (Hucho 1986). The lift force of the wiper is related to its aerodynamic characteristics, which are decided by its shape (Sakoda *et al.* 1986; Toshikazu *et al.* 1983; Michael and Klaus 2009). Nevertheless, the aerodynamic characteristics are not concerned in the design process of most windshield wipers. Therefore, effective methods to analyze and evaluate the aerodynamic characteristics of windshield wipers are urgent to be proposed.

Since sufficient computational resources were not

available at that time, a two-dimensional CFD simulation was conducted by Shibata and Sakoda (1979) to calculate the aerodynamic lift of a wiper model, and the floating concept was first proposed at the same time. Another attempt to study aerodynamic characteristics of the windshield wiper is also based on the two-dimensional numerical simulation (Tsunoda 1983). Hucho (1986) studied the influence of pressure vane angle upon aerodynamic drag and lift of a windshield wiper. As the computing power increases, the aerodynamic characteristics of wipers are studied by three-dimensional numerical simulations in later research. Therefore, further insight into the flow structures around the windshield wiper is provided. Recent references present how aerodynamic lift of wipers changes in various shapes and rotation angles. For example, Harashima and Imamura (2000) studied the influence of the form and angle of fin on aerodynamic lift of the wiper. The aerodynamic effects of various components on the wiping performance were studied (Philippe and Frédéric 2001).

Some efforts, such as the addition of airfoils, spoilers and fins on the wiper blades, to provide additional aerodynamic downward forces to improve the wiper effectiveness were proposed (Walter *et al.* 2007). Sébastien *et al.* (2001) presented the aerodynamic behavior of various configurations of wiper-blades placed on a flat windshield. Seung *et al.* (2011) evaluated the aerodynamic effects of wiping angles and hood tip angle on the wiping performance of the windshield wiper. Based on the computational fluid flow analysis, Ha *et al.* (2013) and Zhang (2011) explained the aerodynamic characteristics of the windshield wiper influenced by the changes of wiper angle and vehicle speed, and the certain angle at which force peaks is found. According to the shape and dimension of the wiper-arm and wiper-blade, and the distance between them, Lin *et al.* (2005) studied the aerodynamic drag and lift of the windshield wiper. Based on the analysis of flow structures around the wipers at different rotational angles, as well as a bare windshield reference case, the effect of wipers on the local flow around the windshield was studied by Gaylard *et al.* (2006). Yang *et al.* (2011) simulated the flow fields around driver side wiper and passenger side wiper at different wiping angles and vehicle speeds separately. The above-mentioned studies offer reasonable results for the design of windshield wipers. However, no relevant experiment was conducted to measure the aerodynamic lift force acting on the windshield wiper, and the influence of the wiping motion upon aerodynamic lift of the wiper was not concerned.

Taking into account above-mentioned problems, aerodynamic lift of four kinds of wipers is tested in the wind tunnel experiment, and the aerodynamic characteristics are studied through relevant steady-state numerical simulations. Besides that, in consideration of the great effects on the airflow taken by the circular motion of wipers, dynamic meshing and user-defined functions (UDF) are used to obtain the transient aerodynamic characteristics of wipers.

2. WIND TUNNEL TEST

2.1 Test Preparation

The test is conducted in the HD-2 wind tunnel at Hunan University, China, which is a low-speed, one-circuit medium-sized boundary layer wind tunnel with two parallel test sections. The current tests were performed in the high speed section, which has a cross-sectional area of $3\times2.5m^2$, and the maximum wind velocity in the test section is 58m/s (Wang *et al.* 2014). In consideration of the experimental conditions in the HD-2 wind tunnel, four kinds of wipers are used, including boneless wiper, A-type three-piece wiper, B-type three-piece wiper and bone wiper, which are noted as wiper A, B, C and D, respectively. Every wiper is 600mm long, which is shown in Fig. 1(a). In order to guarantee the reality and flow quality, the simplified vehicle model is used, which is shown in Fig. 1(b).

a)

b)

Fig. 1. a) Wiper and b) vehicle model.

Force balance can hardly be used to measure aerodynamic lift of the wiper because of its complex layout. Therefore, as is shown in Fig. 2(a), the Multipoint Film Force Test System (MFF) is introduced.

a) b)

Fig. 2. a) MFF and b) film sensors.

The film sensor of this system is just 0.2mm thick with an average error ±0.2N. Considering of the yielding surface contact between the windshield and rubber strip of the wiper, which doesn't meet the measure condition offered by MMF, the strip is replaced by the rigid metal strip with the same shape. And, three film sensors are arranged evenly on the windshield, which is shown in Fig. 2(b). The aerodynamic lift of wipers at a certain wind speed is achieved by subtracting the pressure measured when the wind speed is 0m/s.

2.2 Test Results

In this experiment, for each wiper, the wind speed is 0m/s, 15m/s, 18m/s, 21m/s, 24m/s, 27m/s, 30m/s, respectively, and the rotation angle is 0º, 15º, 30º, 45º, 60º, 75º, 90º, respectively, which is shown in Fig. 3(a). As is shown in Fig. 3(b), the wind speed is tested by hot wire anemometer.

a) b)

Fig. 3. a) Rotation angles and b) hot wire anemometer.

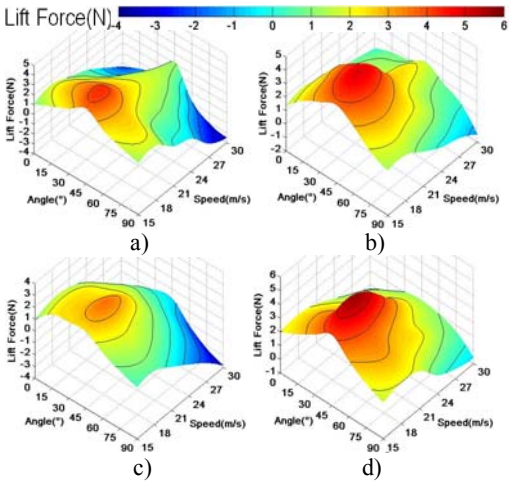

a) b) c) d)

Fig. 4. Aerodynamic lift of a) Wiper A, b) Wiper B, c) Wiper C and d) Wiper D.

The experimental data is fitted into continuous data by using the interp2 functions, which is presented as the three-dimensional graphs in Fig. 4. According to Fig. 4, the aerodynamic lift of each wiper shares the same variation trend. The peak value of aerodynamic lift of each wiper appears under the similar condition, that is, the wind speed is around 18m/s, and the rotation angle is around 45º. At a certain rotation angle, as wind speed increases, the aerodynamic lift increases first and then decreases. From the Fig. 4, obviously, Wiper C holds the best aerodynamic performance. The aerodynamic lift changes smoothly from its maximum value, 3.533N, to minimum value, −3.688N, which is shown in Fig. 4(c). The poorest aerodynamic performance is produced by Wiper D, for aerodynamic lift is generally high with a maximum value, 5.631N.

According to the criterion QC/T44-2009 (2009), a minimum preload force value, 5.4N, is required for the 600-millimeter-long wiper. Thus it can be seen that aerodynamic lift of the wiper takes great effects on its working performance.

3. Numerical Simulation Of Steady-State Aerodynamic Lift

3.1 Simulation Preparation

3.1.1 Geometric Parameters and Boundary Condition

In order to improve the mesh quality and computational efficiency, for each wiper, details with the size below 1 millimeter are simplified, such as the screws, which are shown in Fig. 5. The vehicle model with Wiper C is 2300mm long (L), 970mm high (H) and 1095mm width (W), which is shown in Fig. 6. Based on the HD-2 wind tunnel, the computational domain is set up as a cuboid embracing the model, and the inlet plane starts at a distance of triple the body lengths upstream of the model, while the outlet plane is placed at 7 times its length behind the model. The width and height of the computational domain is 5 times the body width and 7 times the body height, respectively, which gives a blockage ratio of 2.52%, and the blockage effect is eliminated.

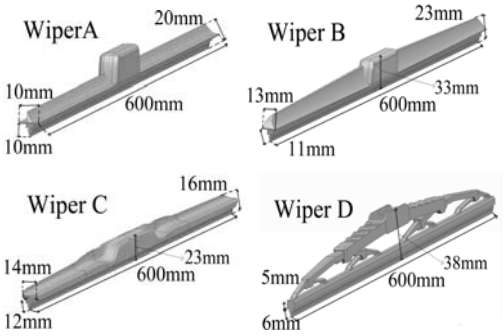

Fig. 5. Wiper model.

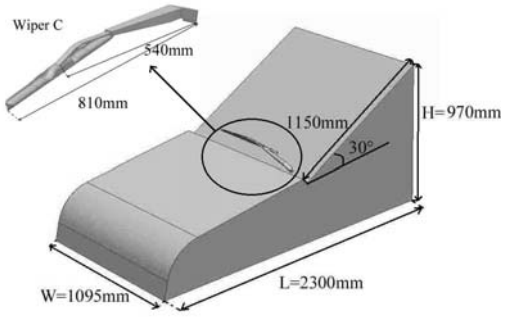

Fig. 6. Vehicle model.

The boundary conditions for the vehicle model, roof and both sides are set up to be no-slip walls, while the floor is treated as a slip wall with the speed of inlet velocity. For the inlet, the velocity-inlet is specified, while the outlet is specified as pressure boundary condition.

Finite volume method is used to create a spatial discretization with the bounded central-differencing scheme. The pressure and velocity are solved in the SIMPLE coupling procedure. The implicit formulation is applied for the spatial terms. According to HD-2 wind tunnel, turbulence intensity of the inlet is set to 0.5% and outlet is set to 5%.

3.1.2 Turbulence Modeling and Grid Independence

In consideration of the transient simulation accuracy in several existing studies (Mehrez *et al.* 2010; Bayraktar 2014; Howard and Pourquie 2002), Large Eddy Simulation (LES) is chosen to be the turbulence model. Filtered Navier-Stokes equations are shown as follows

$$\frac{\partial}{\partial t}\left(\rho\overline{u_i}\right)+\frac{\partial}{\partial x_j}\left(\rho\overline{u_i}\,\overline{u_j}\right)=-\frac{\partial\overline{p}}{\partial x_i}+\frac{\partial}{\partial x_j}\left(\mu\frac{\partial\overline{u_i}}{\partial x_j}\right)-\frac{\partial\tau_{ij}}{\partial x_j} \tag{1}$$

$$\frac{\partial\rho}{\partial t}+\frac{\partial}{\partial x_i}\left(\rho\overline{u_i}\right)=0 \tag{2}$$

Where ρ means fluid density, μ denotes the molecular viscosity coefficient; x_i, x_j means component of the axis, u_i, u_j is the filtered velocity vector. τ_{ij} means the subgrid-scale stress. The sub-grid stress model is given below,

$$\tau_{ij}-\frac{1}{3}\tau_{kk}\delta_{ij}=-2\mu_t\overline{S_{ij}} \tag{3}$$

δ_{ij} means the Kronecker delta, which equals 1 when i=j; otherwise, the value becomes 0. μ_t means the turbulent viscosity and S_{ij} denotes the resolved strain rate tensor.

As is shown in Fig. 7, in view of the complicated geometry of wipers, unstructured grids constructed by tetrahedral and tri-prism mesh are used to discrete the governing equations, and grids near the windshield and wipers are densified.

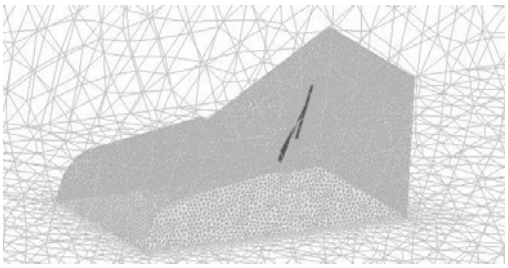

Fig. 7. Mesh of model.

In order to verify the accuracy of LES model, two other widely used turbulence models are introduced, i.e., Detached Eddy Simulation (DES) and Realizable k-ε. And, three computational grids, which include 8.5×10^6, 1.34×10^7 and 2.05×10^7 nodes, respectively, are used to accomplish the computations to achieve the grid independence. The wall normal resolution y+ <1 is achieved by all above mentioned three computational grids. Case based on the certain grid and turbulence model is presented in Table 1.

Table 1 Various cases based on the different turbulence models and grids.

model / grid	LES	DES	Realizable k-ε
$8.5\text{x}10^6$	case 1	case 4	case 7
$1.34\text{x}10^7$	case 2	case 5	case 8
$2.05\text{x}10^7$	case 3	case 6	case 9

For Wiper C at a 45-degree rotation angle with a wind speed of 18m/s, based on DELL Power 32 processors, the aerodynamic lift and computing time based on various cases are shown in Table 2. It can be concluded that case 2, which is based on LES and the grid including 1.34×10^7 nodes, gives the reasonable prediction without consuming significant computational resources. Consequently, the case, which is based on LES and the grid including 1.34×10^7 nodes, is believed to be fine enough to give all reasonable results in this paper.

Table 2 Aerodynamic lift and computing time based on various cases.

case	aerodynamic lift	e (%)	Computing time (h)
case 1	3.227	8.06%	3.5
case 2	3.241	7.66%	6
case 3	3.239	7.72%	14.5
case 4	3.855	9.83%	3
case 5	3.824	8.95%	4.5
case 6	3.822	8.89%	12
case 7	3.843	9.49%	2
case 8	3.792	8.03%	3.5
case 9	3.794	8.09%	8
experiment	3.510	——	

3.2 Results and Discussion

Each wiper is tested at a 45-degree rotation angle with a wind speed of 15m/s, 18m/s, 21m/s, 24m/s, 27m/s, 30m/s, respectively, and at a wind speed of 18m/s with a rotation angle of 0º, 15º, 30º, 45º, 60º, 75º, 90º, respectively. Fig. 8 presents the evolution of aerodynamic lift of each wiper at a 45-degree

rotation angle with the change of wind speeds. The results are consistent with the wind tunnel experimental data. It can be concluded that the simulation strategy used here is reasonable.

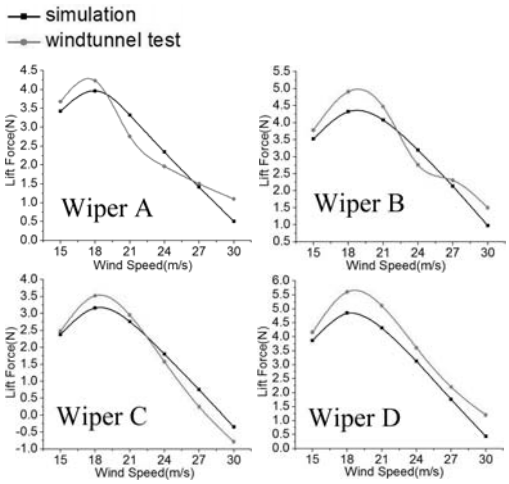

Fig. 8.Steady-state aerodynamic lift at different wind speeds.

The static pressure distribution on the surface of wiper C at the 45-degree rotation angle with a wind speed of 21m/s is presented in Fig. 9. Static pressure on the upper surface and lower surface is 2.124N and 4.883N, respectively, which is calculated by integrals. The rubber strip and bracket together form a T-shape structure, which forms a groove in combination with the windshield. High-speed air flow is blocked in the groove, so the pressure acting on the lower surface is higher.

Figure 10 shows the evolution of aerodynamic lift of each wiper at a wind speed of 18m/s with the change of rotation angles. The results at a wind speed of 70km/h achieved by Yang *et al.* (2011) are introduced as a comparison. The value of aerodynamic lift of each wiper peaks around the 45-degree rotation angle. The numerical results are consistent with the experimental data. The change trend of aerodynamic lift achieved here coincides well with the results calculated by Yang *et al.* (2011) and other related references (Seung *et al.* 2011). The deviation of the magnitude is due to the different configurations of wiper-blades.

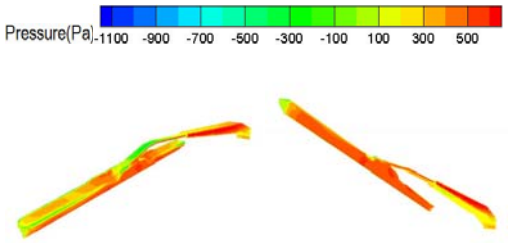

Fig. 9. Static pressure distribution on the wiper.

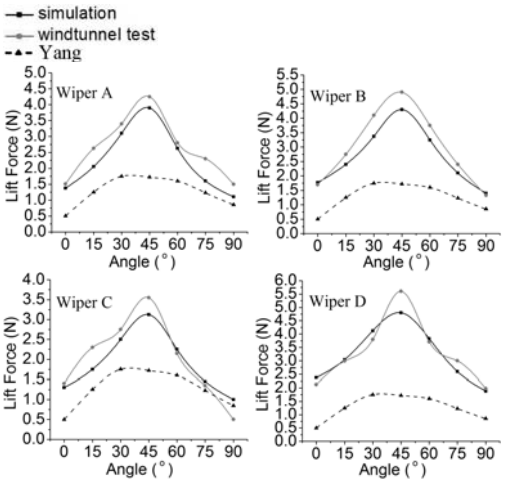

Fig. 10. Steady-state aerodynamic lift at different rotation angles.

Streamlines around wiper C with a rotation angle of 15º, 30º, 45º, 60º, respectively, are shown in Fig. 11. The wiper at a small rotation angle is markedly affected by the low velocity zone formed at the border of the windshield and hood. The average wind speed upon the windward of wiper C at the 15-degree and 30-degree rotation angle is 7.5m/s and 12.5m/s, respectively. According to Fig. 11(a) and Fig. 11(b), the helical vortex behind the wiper at a rotation angle of 15º is smaller than 30º, which explains why the aerodynamic lift increases as the wiper rotates from zero to 45 degrees. The size of helical vortex remains stable after the rotation angle reaches 45 degrees, which is shown in Fig. 11(c) and Fig. 11(d). As the angle between the airflow and wiper decreases, effective windward area of the wiper reduces, and air flows through the wiper more smoothly.

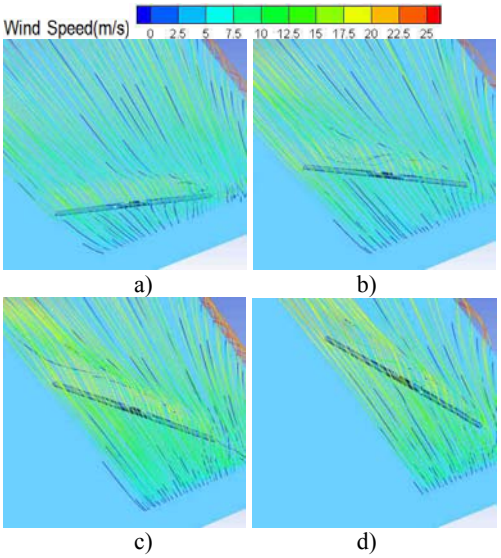

Fig. 11. Streamlines around Wiper C at the rotation angle of a) 15º, b) 30º, c) 45º and d) 60º.

4. NUMERICAL SIMULATION OF TRANSIENT AERODYNAMIC LIFT

4.1 Moving Mesh

The same grid is used to discrete the governing equations, and moving mesh conservation equation is followed to avoid the extraneous errors produced by mesh motion. Moving mesh update methods include the elastic deformation and local remeshing method. For each control volume V with the movement-boundary, the balance equation of the scalar φ is:

$$\frac{d}{d_t}\int_V \rho\varphi dV + \int_{\partial V} \rho\varphi\left(u - u_g\right)\bullet dA = \int_{\partial V} \Gamma\nabla\varphi \bullet dA + \int_V S_\varphi dV \quad (4)$$

u_g means the moving speed of the mesh, Γ denotes the diffusion coefficient; $S_\square$ is a source term of φ, ∂V is the boundary of control volume V, u is the velocity vector and ρ means fluid density.

In consideration of grid quality problems produced by complicated surfaces of the wiper, the simplified moving domain is proposed, which is shown in Fig. 12. The simplified domain embracing the wiper guarantees the grid quality by avoiding the deformation and remeshing of adjacent grids close to the wiper, and reduces the amount of remeshing units, which also improves the efficiency greatly. As is shown in Fig. 13, the grid aberration with a simplified domain is less serious, especially close to the wiper, which improves the calculation accuracy greatly.

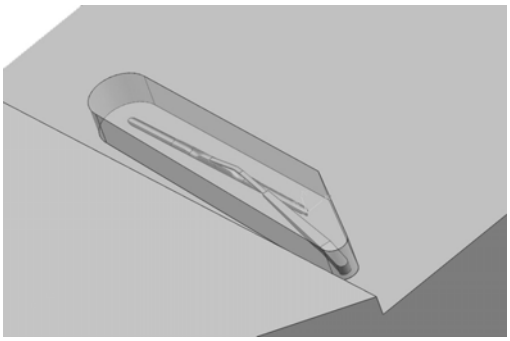

Fig. 12. Wiper C with the simplified moving domain.

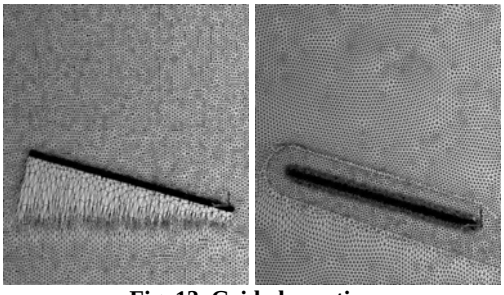

Fig. 13. Grid aberration.

The mesh on the windshield is defined as deforming, and the simplified domain embracing the wiper is defined as a rigid body. For the rigid body, origin position is regarded as the rotation angle of 0º, the speed of rotation is 1.5 rad/s. The rigid body rotates with the free stream by 90 degrees, and then enters a 0.3 seconds of stagnation. After that, the rigid body rotates against the free stream to origin position, and then enters another stagnation lasting 0.5 seconds. With this, one cycle ends and another cycle comes. The mesh motion is implemented by using user-defined functions (UDF), the coding is as follows:

```
for (i=0; i<=n; i++)
        {if (2i<time<2i+1.05)
            omega[0]=1.5; \\ rotate with the
                                free stream
            else if (2i+1.35<time<2i+2.4)
            omega[0]=−1.5; \\ rotates against the
                                free stream
          else
            omega[0] =0 \\stagnation}
```

4.2 Results and Discussions

Figure 14 shows the change trend of steady and transient aerodynamic lift of Wiper C at a wind speed of 18m/s as the angle changes. It presents that the aerodynamic lift acting on Wiper C with downstream rotation is generally lower than steady, and the value with upstream rotation is generally higher than steady. The gaps are more obvious when the angle is between 0 degree and 45 degrees.

Streamlines and velocity contour at four typical planes (see Fig. 15 for the location of the planes) are shown in Fig. 16. The wiper rotating downstream experiences weaker interactions with the airflow. The air flows through the wiper smoothly, and the velocity contours are equally distributed, which is shown in Fig. 16. The airflow behind the wiper rotating against the free stream deflects largely. And then, low-pressure area forms behind the wiper, and the flow upon the wiper is inhaled. A vortex forms behind the wiper, which aggravates the pressure differential between upper and lower surface of the wiper.

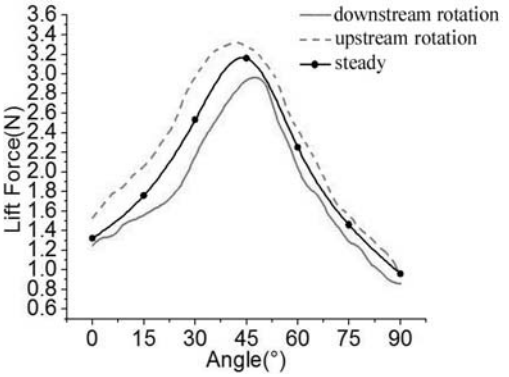

Fig. 14. The variation of aerodynamic lift as rotation angle changes.

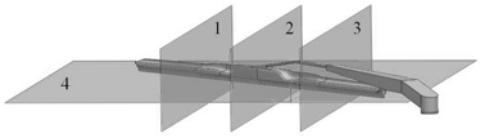

Fig. 15. Plane location for streamlines.

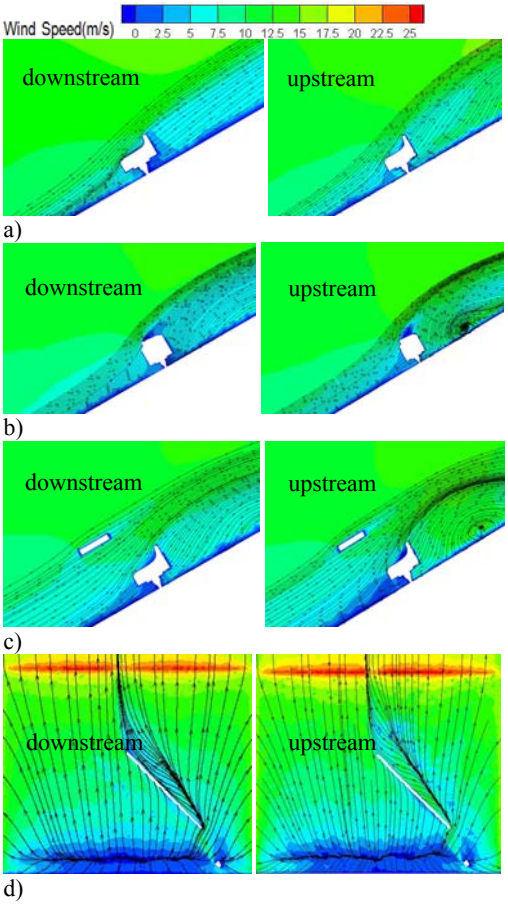

Fig. 16. Streamlines and velocity contour at plan a) 1, b) 2, c) 3 and d) 4 when the wiper is rotating downstream and upstream.

Static pressure on the windshield when the wiper is rotating downstream and upstream are presented in Fig. 17. When the wiper is rotating upstream, the pressure and pressure gradient are generally higher, which verifies that more acute interaction with the airflow is produced by the wiper rotating upstream. From Fig. 17, static pressure gradient on the windshield is extremely high when the wiper rotates to 45 degrees, which explains that the value of aerodynamic lift acting on each wiper peaks around the 45-degree rotation angle.

5. CONCLUSION

Aerodynamic characteristics of four kinds of wiper are studied through the experiment and numerical simulation. It can be concluded that the wiper's aerodynamic characteristics have great effects on its working performance, the conclusions are detailed as follows.

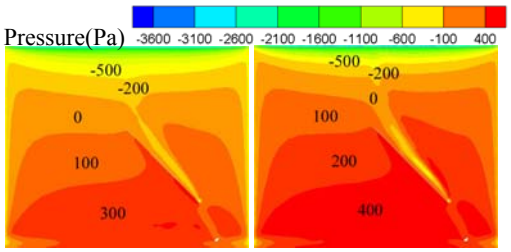

Fig. 17. The static pressure on the windshield when the wiper is rotating a) downstream and b) upstream.

(1) For the experimental model, aerodynamic lift counteracts the preloaded pressure by 68% at most. The change rule of the aerodynamic lift of each wiper is roughly similar, that is, the peak value appears when wind speed is around 18m/s and the rotation angle is around 45º.

(2) The numerical results are consistent with the experimental data. The change trend of aerodynamic lift achieved here coincides well with early studies.

(3) The wiper motion has a great effect on the nearby flow field, and the aerodynamic characteristics are presented accurately by the transient numerical simulation. Aerodynamic lift of the wiper rotating upstream is higher than steady, and the value with downstream rotation is lower than steady.

(4) By comparing the results achieved by above methods with early studies, reasonable results of the aerodynamic characteristics of windshield wipers are achieved, which can be widely integrated into the vehicle design and performance analysis.

ACKNOWLEDGEMENTS

The aerodynamic characteristics of a wiper are influenced by many factors, such as the shape of the wiper and vehicle, rotational frequency and water film covering the wiper and windshield, which will be discussed in the future research. This work was supported by the National Natural Science Foundation of China under Grant No. 50975083; National Hundred, Thousand, and Ten Thousand Talent Program of Ministry of Transport of China under Grant No. 20120222; Independent Subject of State Key Laboratory of Advanced Design and Manufacturing for Vehicle Body under Grant No.734215002; and Innovation Team of Ministry of Finance of China under Grant No.0420036017.

REFERENCES

Ali, Z., N. Amin, Z. M. Z. Mohd and R. A. B. Abd (2013). Practical multi-objective controller for preventing noise and vibration in an automobile wiper system. *Swarm and Evolutionary Computation* 8, 54-68.

Anderson, M. (1903). Window-cleaning device. Patent No. 743,801, United State Patent Office.

Bayraktar, S. (2014). Numerical solution of three-dimensional flow over angled backward-facing step with raised upper wall. *Journal of Applied Fluid Mechanics* 7(1), 155-167.

Dongki, M., J. Seongbin, H. Y. Hong, K. Heewon and P. Junhong (2014). Experimental investigation of vehicle wiper blade's squeal noise generation due to windscreen waviness. *Tribology International* 80, 191-197.

Frédéric, B., B. Roland, L. Vincent, P. Maria, L. Sophie, C. Viola and C. Michèle (2014). Measuring the effect of the rainfall on the windshield in terms of visual performance. *Accident Analysis and Prevention* 63, 83-88.

Gaylard, A., A. C. Wilson and G. S. J. Bambrook (2006, October). A quasi-unsteady description of windscreen wiper induced flow structures. *6th MIRA International Conference on Vehicle Aerodynamics*, Gaydon, United Kingdom.

Ha, J. S., T. K. Kim, K. H. Kim, K. W. Kim and Y. K. Chang (2013). A study on the lift characteristics according to the change of blade angle in car wiper. *Journal of Korean Society of Mechanical Technology* 15(1), 27-31.

Harashima, M., A. Masuda and S. Imamura (1997). Effect of fin on the wiper lift characteristics in high-speed. *Journal of the Visualization Society of Japan* 17(2), 19-22.

Howard, R. J. A. and M. Pourquie (2002). Large eddy simulation on the Ahmed reference model. *Journal of Turbulence* 3(12), 1-18.

Hucho, W. (1986). *Aerodynamics of Road Vehicles (First Edition)*. Cambridge University Press, Cambridge, UK.

Lin, C. F., M. F. Hung, C. Y. Tseng, C. H. Tsai, C. H. Tai and C. C. Lan (2005). Numerical investigation of aerodynamic effects on windshield wiper. *Journal of Technology* 20(4), 325-332.

Mehrez, Z., M. Bouterra, A. E. Cafsi, A. Belghith and P. L. Quéré (2010). Simulation of the periodically perturbed separated and reattaching flow over a backward-facing step. *Journal of Applied Fluid Mechanics* 3(2), 1-8.

Michael, P. U., and A. H. Klaus (2009). Computations of Turbulent Flow over an Aircraft Windshield Wiper Model. *AIAA Journal* 2009-3977.

Philippe, B., J. Sébastien, and M. Frédéric (2001). Simulation of aerodynamic uplift consequences on pressure repartition – application on an innovative wiper blade design. *SAE Paper* 2001-01-1043.

Sakoda, Nakagawa and Kameyama (1986). Visualization technology of automobile aerodynamic. *Flow Visualization* 6(21), 256-274.

Sanon, A. and S. Jallet (2003). Acoustic sources localization: Application to wiper aerodynamic noises. *SAE Paper* 2003-01-1700.

Sébastien, J., D. Sylvain, M. Daniel, S. Jean, M. Frédéric and D. Thomas (2001). Numerical simulation of wiper system aerodynamic behavior. *SAE Paper* 2001-01-0036.

Seung, H. L., W. L. Sung, H. L. Sang, N. C. Woo and H. S. Jin (2011). Numerical study on aerodynamic lift on windshield wiper of high-speed passenger vehicles. *Transactions of the KSME—B* 35(4), 345-352.

Shibata and Sakoda (1979). Research on the automobile wipers floating. *Automobile Technology Academic Lectures* 791, 124-156.

Takada, K., T. Komoriya and Y. Furugori (2003). Numerical simulation of wiper blade uplifting on high speed traveling. *The Japan Society of Mechanical Engineers* 38, 38-39.

Toshikazu, S., S. Masanori and N. Kunio (1983). A study on aerodynamic characteristics of passenger cars. *SAE Paper* 1983-11-07.

Tsunoda (1984). The aerodynamic characteristics of automobile wipers. *Automobile Technology Academic Lectures* 842, 039-052.

Walter, W. C., K. Steve, D. Thomas, G. H. Daryl and J. Sébastien (2007). Wiper blade assembly and method of forming the same. Pub. No.: US 2007/0017056 A1, Patent Application Publication, United States.

Wang, Y., Y. Xin, Z. Q. Gu, S. H. Wang, Y. Deng and X. Yang (2014). Numerical and experimental investigations on the aerodynamic characteristic of three typical passenger vehicles. *Journal of Applied Fluid Mechanics* 7(4), 659-671.

Yang, Z. G., X. M. Ju and Q. L. Li (2011). Numerical analysis on aerodynamic forces on wiper system. *Recent Progress in Fluid Dynamics Research* 1376, 213-217.

Zhang, J. H. (2010). *Numerical simulation of the aerodynamic wiper on high-speed locomotives based on FLUENT*. Ph. D. thesis, Southwest Jiaotong University, Cheng Du, China.